THE JOURNAL OF PHYSICAL CHEMISTRY C
A JOURNAL OF THE AMERICAN CHEMICAL SOCIETY

pubs.acs.org/JPCC
Article

Electronic Properties of Hexagonal V-Shaped Gallium Nitride Pits

Vladimir Miranda La Hera,[§] Josué Mena,[§] Esdras Josué Canto-Aguilar, Hamid Reza Barzegar, Joan J. Carvajal, Thomas Wågberg,* and Eduardo Gracia-Espino*

Cite This: J. Phys. Chem. C 2023, 127, 24658−24665
Read Online

ACCESS | Metrics & More | Article Recommendations | Supporting Information

ABSTRACT: In this work, the morphology, surface composition, and electronic properties of porous GaN films containing hexagonal V-shaped pits were studied. The V-pits are orientated along the [0001] direction of GaN, and we observed a clear relation between the growth time with the surface composition, film thickness, and pit morphology, which in turn had a significant impact on the band gap, valence band maximum, and the work function. The effect on the position of the valence band maximum and work function is explained by the formation of superficial oxygen-rich phases such as Ga_2O_3 and nonstoichiometric GaN_xO_y as supported by X-ray photoelectron spectroscopy and density functional theory (DFT). We further show a change in the optical band gap with the thickness of the porous films explained by a change in the tensile strain caused by open-core screw dislocations that gives rise to the formation of V-pits. The correlation between strain and the band gap is supported by DFT calculations. Our study provides insights into the intricate relation between surface states and electronic properties of semiconducting materials and offers directions for designing GaN heterojunctions with specific optical and electronic properties.

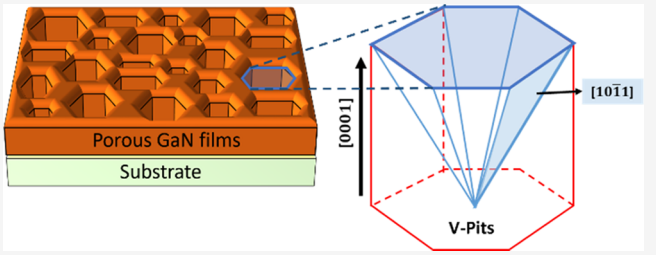

INTRODUCTION

Gallium nitride is an interesting semiconductor material from the III−V group which in recent years has gained considerable attention due to its vast use in the fabrication of bright light-emitting diodes, laser diodes, high-power/high-temperature electronics, as well as in photoelectrocatalysis.[1−3] When prepared in a porous form, GaN often shows enhanced specific surface area, optical activity, luminescence efficiency,[4] and unique electronic properties, as well as lower optical reflectance[5] and tunable refractive index[6] when compared with their flat counterparts. These enhanced features are desired when developing state-of-the-art reflective/refractive materials and high-efficiency photoelectronics and photochemical conversion devices. All these significantly increase the applicability of porous GaN in photonic-based technologies.[6] Another advantage of porous GaN relates to the relaxation of the stress generated at the substrate/GaN interface due to lattice constant mismatch.[7] The reduced stress can have a positive effect on devices by minimizing their degradation performance.

Several techniques have been used to grow and deposit GaN films, such as sublimation,[8] molecular beam epitaxy,[9] and chemical vapor deposition (CVD),[10] just to mention a few. The main advantages of using CVD over other techniques rely on controlling the reaction environment leading to the production of large-scale uniform films with high purity and stability.[11,12] In addition, polycrystalline GaN films can be deposited via CVD, resulting in nanoporous GaN coatings with V-pits that exhibit interesting antireflective properties suitable for a variety of technologies.[13,14] In addition, there is a clear correlation between the film growth kinetics and the resulting surface morphology and density of pores.[15−17] These pits exhibit different properties than flat surfaces, acting as favorable oxygen traps that can modify the electronic and optical properties.[18−22] In addition, the existence of a biaxial strain in CVD-grown GaN epitaxial layers and possible changes in surface composition can cause alterations in its band structure. Therefore, it is required to investigate how changes in film morphology and surface composition affect electronic properties such as work function, Fermi-level pinning, and electronic surface states, among others.

In this work, we investigate the correlation that surface composition, film thickness, and lattice strain have over the optical band gap, work function, and valence band maximum of porous GaN films containing a high density of hexagonal V-shaped pits. We discuss the formation of oxygen-rich phases on exposed crystallographic surfaces inside the V-pits with high oxygen affinity and associate these to an unintentional *n*-doped behavior. We also observed a correlation between biaxial lattice strain in porous GaN and the optical band gap.

Received: August 31, 2023
Revised: December 4, 2023
Accepted: December 5, 2023
Published: December 14, 2023

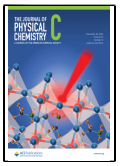

https://doi.org/10.1021/acs.jpcc.3c05878
J. Phys. Chem. C 2023, 127, 24658−24665

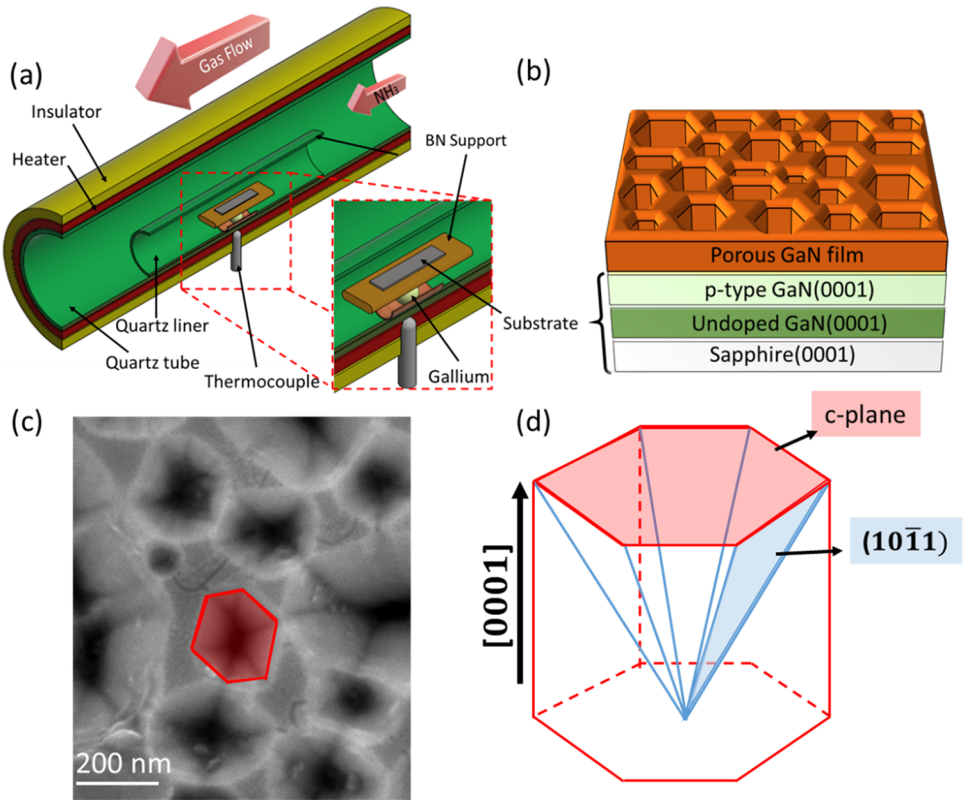

Figure 1. (a) Schematic representation of the CVD setup used to grow porous GaN. (b) Schematic representation of the multilayered substrate (sapphire/GaN/*p*-type GaN) with the epitaxially grown porous GaN film with V-pits. (c) SEM micrograph of the porous GaN (60 min deposition time) where the highlighted area indicates the hexagonal V-pits. (d) Growth direction and crystalline facets that constitute the V-pits.

METHODS

Materials Growth. Porous GaN was grown via CVD by direct reaction between metallic Ga and NH_3 gas, as reported elsewhere.[23] Briefly (and shown in Figure 1a), a substrate consisting of 1 μm-thick *p*-type GaN(0001) doped with Mg/3 μm-thick undoped GaN(0001)/sapphire(0001) was placed facing the Ga droplet on a boron nitride (BN) support with a window of approximately 0.7 × 0.7 cm^2. The substrate was placed above the window with a vertical distance of 1.7 cm. The entire setup was placed at the center of a 2 in.-diameter quartz tube CVD tubular furnace (Thermolyne 79300). Prior to the growth, the system was purged by degassing to a pressure below 10^{-2} Torr. NH_3 was introduced at a flow rate of 75 sccm using a mass-flow controller; the flow was kept throughout the experiment while keeping the pressure at 15 Torr. Afterward, the furnace was heated to a temperature of 930 °C by using a heating rate of 60 °C·min^{-1}. The deposition time was varied (15, 30, 45, and 60 min) for every experiment. Finally, the growth was stopped by switching off the furnace and the NH_3 flow, and the system was let to cool to room temperature under a pressure of ~10^{-2} Torr.

Material Characterization. The morphology of the porous GaN was studied with a scanning electron microscope (Carl Zeiss Merlin FESEM), using the detector In-lens and with an electron high tension (EHT) of 5 kV. The optical band gaps were obtained via diffusive reflectance measurements using an Agilent Cary 5000 UV−vis-NIR spectrophotometer equipped with an internal diffuse reflectance accessory (DRA) integrating sphere. X-ray photoelectron spectroscopy (XPS) was carried out using an AXIS Ultra DLD electron spectrometer manufactured by KRATOS Analytical LTD with a monochromatic source Al Kα-line (1486.6 eV) and a pass energy of 20 eV. The high-resolution spectra were obtained using an energy step of 100 meV. Ultraviolet photoelectron spectroscopy (UPS) measurements were performed using an ARPES Scienta R3000 hemispherical electron analyzer manufactured by VG SCIENTA equipped with an ultraviolet light source with He gas, including two photon energies (21.2 eV (He−I) and 40.8 eV (He−II)). A schematic of the ultrahigh vacuum (UHV) system is seen in Figures S1 and S2. Prior to the UPS measurements, all samples were stored under UHV conditions for at least 12 h, and then the samples were annealed at 800 °C for 5 min to remove any contamination or adsorbed species. Afterward, the UPS measurements were performed at room temperature. The UPS was calibrated at room temperature using a pass energy of 5 eV resulting in a resolution of 4.8 meV, as determined by the width of the Fermi edge measured on a Mo substrate. The obtained binding energy (BE) values refer to the Fermi level. The UPS spectra were measured at a normal emission geometry with an acceptance angle of 10°, a slit width of 1.3 mm, and an energy step size of 3.98 meV. A pass energy of 10 eV was used during measurements which reduced the resolution to 9.9 meV. The work function values were determined from the secondary electrons cutoff spectra measured under a bias of −5 V. A complete list of parameters used during the UPS measurements is found in Table S1.

Computational Details. The computational studies were performed using density functional theory (DFT) as implemented in the Quantum Espresso code.[24,25] We used the Perdew−Burke−Ernzerhof (PBE) implementation as the exchange-correlation functional. Norm-conserving pseudopo-

https://doi.org/10.1021/acs.jpcc.3c05878
J. Phys. Chem. C 2023, 127, 24658−24665

tentials (PPS) were constructed with the Martins-Troullier approach.[26] The systems were geometrically optimized until the components in the atomic forces were less than 1×10^{-3} (a.u.), and the total energy change was less than 1×10^{-4} (a.u.). A kinetic energy cutoff for wave functions of 120 Ry was used, and 480 Ry of kinetic energy cutoff for the charge density and potential. The Brillouin zone was sampled using an $8 \times 8 \times 8$ k-grid for bulk systems, while an $8 \times 8 \times 1$ was used for surfaces. No spin polarization was considered. After geometrical relaxation, the electronic structure was evaluated using the hybrid Heyd–Scuseria–Ernzerhof (HSE)[27] approach as exchange-correlation functional with a mixing parameter α of 0.25. A q-grid of $2 \times 2 \times 2$ was used to sample the Fock operator. All other parameters remained unchanged.

RESULTS AND DISCUSSION

Surface Morphology. Porous GaN films were grown by direct reaction between NH_3 gas and metallic Ga in a CVD setup as schematically shown in Figure 1a. A quartz boat with metallic Ga was placed below a BN support with an opening window of 0.7×0.7 cm^2. On top of the BN support, a multilayered p-type GaN substrate (depicted in Figure 1b) was placed facing down the metallic Ga. The entire construction was placed inside a quartz liner that sits inside a wider quartz tube with a controlled atmosphere (more details in the experimental section).

Porous GaN grows epitaxially from the underlying p-doped GaN (0001) substrate, and the formation of V-pits is controlled by varying the growth time from 15 to 60 min. SEM studies reveal that the pits exhibit a distorted hexagonal shape, as depicted in Figure 1c, aligned along the [0001] crystallographic direction of GaN, while the side walls consist of $(10\bar{1}1)$ GaN surfaces (see Figure 1d). Similar V-pits in GaN were reported by Heying et al. using plasma-assisted molecular beam epitaxy. The reported pits are formed by six $\{10\bar{1}1\}$ planes that started to merge when the density of the pits increased,[28] in agreement with our observations. All samples produced at different growth times (15–60 min) exhibited V-pits spread along the surface; however, the pit's size and distribution, as well as the porous GaN film thickness, are strongly influenced by the deposition time.

Figure 2 shows SEM images for samples obtained at different growth times. From these micrographs, two main characteristics are evident: (1) The presence of faceted particles along the surface. (2) The appearance of small pores in addition to the large distorted hexagonal V-pits. As shown in Table 1, the V-pit size evaluated from SEM images increases from 104 to 246 nm as the growth time increases from 15 to 45 min, in good agreement with AFM measurements (Table S2). The size correlation with growth time indicates that the V-pits merge as the thickness of the porous GaN increases, decreasing their spatial density at longer growth times. Finally, an increase in the thickness of the porous GaN layer is observed from 0.5 (15 min) to 1.7 μm (60 min), as summarized in Table S2.

Note that the V-pits diameter (Table 1) reaches a maximum value of ~250 nm at 45 min (Figure 2e) of growth time. This suggests that longer growth times lead to a thickening of the pit walls, which is seen as a reduction in diameter. This is evidenced from Figure 2f (60 min) where the space between V-pits is increased when compared to Figure 2e (45 min). At all growth times, faceted particles are apparent on the surface along with the pits (Figure 2a–f).

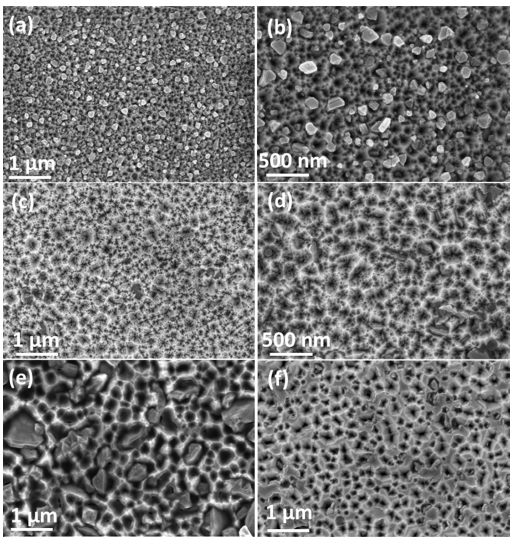

Figure 2. SEM micrographs of porous GaN at (a, b) 15, (c, d) 30, (e) 45, and (f) 60 min of growth time.

Table 1. Average V-Pits Diameter at Different Growth Times

growth time (min)	average V-pits size (nm)
15	104 ± 30
30	223 ± 39
45	246 ± 53
60	196 ± 48

Electronic Properties. We studied the electronic properties of the porous GaN by evaluating their optical band gap (E_g) using diffuse reflectance spectroscopy and their valence band maximum (VBM) and work function (Φ_S) using ultraviolet photospectroscopy (UPS). The optical band gap was evaluated at room temperature from Tauc's plots in Figure S3, and the results are summarized in Figure 3. As a reference, E_g of the clean multilayered p-type-GaN/undoped-GaN/sapphire substrate was equal to 3.37 eV. The porous GaN films exhibited E_g values ranging between 3.32 and 3.34 eV. These values differed by a few meV when compared to homoepitaxially grown GaN with a reported band gap of 3.40 eV.[29] The energy difference can be attributed to surface defects, structural strain due to the presence of V-pits, as well as lattice strain generated by the lattice mismatch between the grown sample and the substrate or by the presence of defects and dislocations. However, it has been reported that the growth of GaN on sapphire substrates results in a compressive biaxial strain due to the lattice mismatch and differences in thermal expansion coefficients.[29,30] In our case, the GaN substrate contains an intermediate 3 μm undoped-GaN layer between the sapphire and the p-type GaN layer with the aim to minimize the compressive strain caused by the sapphire substrate. Therefore, the observed tensile strain in our samples must have a different origin. It has been reported that GaN grown by molecular beam epitaxy under Ga-rich conditions experiences a formation of open-core screw dislocations resulting in the formation of pits.[31] The latter indicates that the observed residual tensile strain could arise from the center of the V-pits by inducing biaxial stress, in which the formation of the V-pits is a mechanism to stabilize the energy of the system by forming more energetically favorable surfaces.[32] By

https://doi.org/10.1021/acs.jpcc.3c05878
J. Phys. Chem. C 2023, 127, 24658–24665

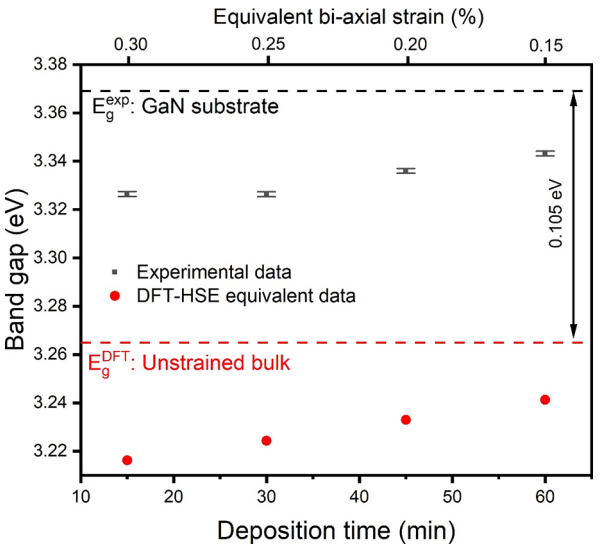

Figure 3. Experimental optical band gap as a function of growth time and DFT-HSE simulated electronic band gap as a function of biaxial strain. The black dashed line represents the experimental E_g of the strain-free *p*-type-GaN/undoped-GaN/sapphire substrate. The error bars were obtained from the linear fit performed in Tauc's plot, Figure S3. The red dashed line is the electronic E_g of the unstrained GaN bulk evaluated by DFT-HSE.

comparing E_g of our samples to a strain-free grown GaN (3.40 eV),[29] we can see deviations as large as ∼0.08 eV for the porous GaN films, while for the *p*-type GaN layer, the difference was only ∼0.03 eV. The larger deviation seen on porous GaN suggests an additional accumulation of strain likely caused by the presence of open-core screw dislocations which produces the V-pits.

The change in electronic band gap due to the presence of tensile strain in GaN was corroborated by theoretical calculations using DFT with the hybrid HSE functional.[27] We evaluated the evolution of the electronic band gap by introducing a biaxial tensile strain, as experimentally reported for GaN grown on sapphire.[29,33,34] Eight different biaxial strains up to 1.01% were evaluated, and in this range, we observed a perfect linear correlation between the band gap and the induced strain (see Figure S4). A theoretical band gap of 3.27 eV was obtained which is in excellent agreement with other theoretical studies.[35−37] The observed changes in band gap are in line with previous studies reported by Chatzopoulou et al.[38] in which E_g decreased 5.4% (3.28 to ∼3.1 eV) when applying a 1.5% biaxial strain. In comparison, we observed a reduction of 7.4% for a similar biaxial strain. These calculations provide an opportunity to estimate the strain in our samples by comparing the optical band gap to the theoretical electronic band gap. We have done this by evaluating the relative change in the band gap seen experimentally, which is in the range of −1.28 to −0.78% for films grown for 15 to 60 min, respectively. A similar change in E_g is found for strain in the range of 0.30 to 0.73% as seen from Figure 3, where clear similarities can be observed. Note that all E_g evaluated from the DFT-HSE simulations are underestimated by 0.105 eV due to an incomplete description of the electronic structure by DFT.[39] The value at zero strain is compared to the experimental value of 3.37 eV (indicated by the black dashed line) of the multilayered *p*-type-GaN/undoped-GaN/sapphire substrate. With these results, we can conclude that the increase in optical band gap seen in samples produced at longer growth times corresponds with a reduction in biaxial strain, as previously discussed.

The valence band maximum was experimentally identified by UPS using two different photo energies (He−I and He−II). The corresponding UPS spectra are shown in Figures S5−S8, from which the VBM was evaluated using the expression VBM = $\Delta(E_V - E_F)$. The Fermi level (E_F) was taken from the position of the previously calibrated detector as explained in the Experimental section, while the valence band energy (E_V) corresponds to the position of the cutoff at the lowest BE side (∼0 eV region) as obtained from Figures S5 and S6. From these, two different VBM values are obtained when using He−I (21.21 eV) and He−II (40.81 eV) (see Figure 4). The

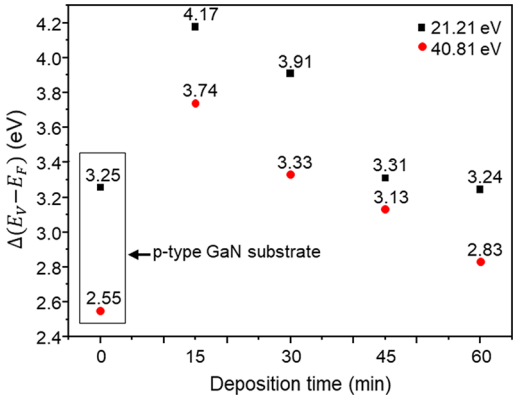

Figure 4. VBM position obtained with two different light sources, He−I and He−II, for samples produced at different growth times. The box indicates the values corresponding to the *p*-type-GaN/undoped-GaN/sapphire substrate.

difference is explained by the so-called information depth from which the photoemitted signal originates. Here, the He−I excitation is significantly more sensitive to the surface with an inelastic mean free path (IMFP) in GaN of ∼2 Å, compared to the ∼5 Å IMFP of He−II.[40,41] From Figure 4, we can see that there is a difference of 0.7 eV between the two values of VBM for the GaN substrate obtained with He−I and He−II light sources. The larger VBM from He−I measurements suggests an *n*-type behavior of the GaN substrate, which is contrary to what is expected since the substrate is a *p*-type semiconductor. However, the He−II measurements show a more dominant *p*-type behavior due to its higher penetration depth. This discrepancy can be caused by superficial morphological changes and the presence of surface contaminants.[42]

Φ_S was determined from the lower cutoff UPS spectra, using $\Phi_S = h\nu - E_{cutoff}$, using the incident photon energy ($h\nu$) of 40.81 eV from the He−II, and E_{cutoff} from the spectrum cutoff at the higher BE side (∼36 eV region) is shown in Figures S7 and S8. The ionization energy (IP) can thereby be determined by using IP = Φ_S + VBM. Calculated values for VBM, Φ_S, and IP are represented in the energy diagram referenced to the vacuum level (VL) as shown in Figure 5. By taking advantage of the larger penetration depth of the He−II source, the contribution of surface contaminants is minimized.

For the multilayered GaN substrate, values of 2.55 and 4.26 eV were observed for VBM and Φ_S, respectively. These results can be rationalized by considering that the presence of hydrocarbons and oxygen/hydroxide species can shift the VBM by several eV below the Fermi level resulting in an

https://doi.org/10.1021/acs.jpcc.3c05878
J. Phys. Chem. C 2023, 127, 24658−24665

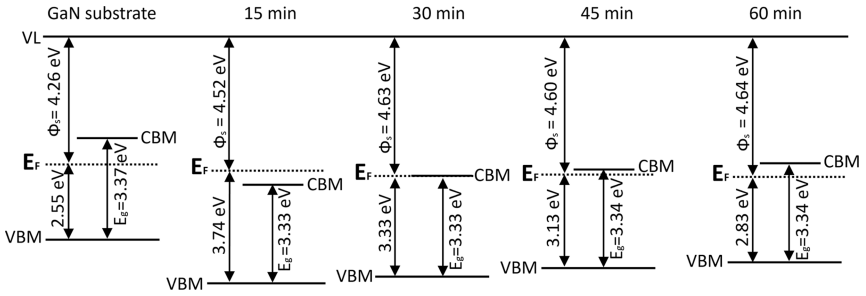

Figure 5. Energy diagram aligned to the VL for samples produced at different growth times. These values were obtained using He−II as the excitation source. CBM, VBM, and E_F represent the conduction band minimum, valence band maximum, and the Fermi level, respectively.

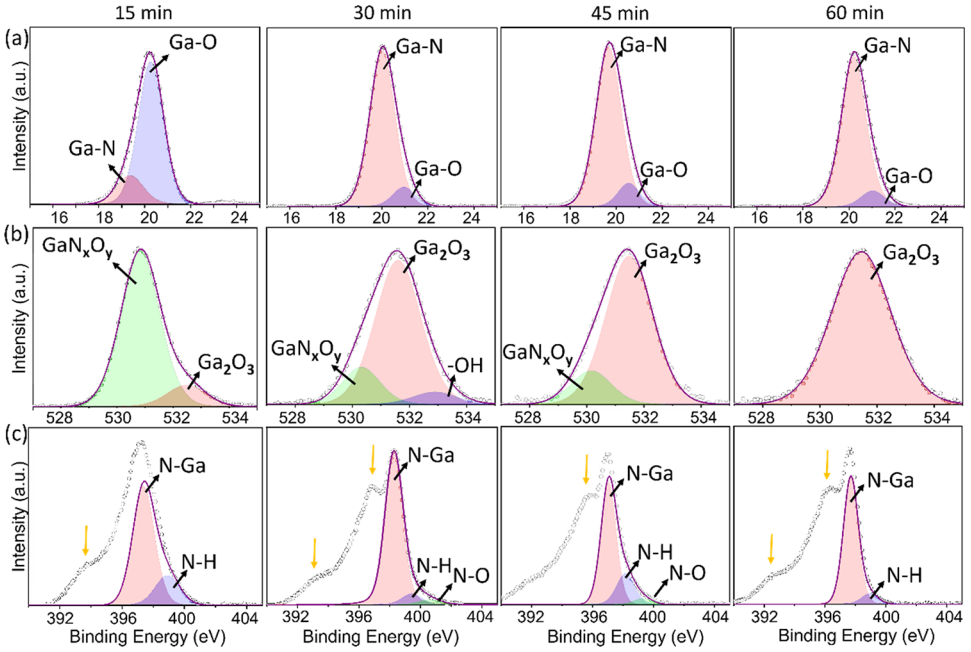

Figure 6. XPS deconvolution of states in the (a) Ga (3d), (b) O (1s), and (c) N (1s) spectra for samples at different growth times.

apparent *n*-type behavior, as reported by Tracy and coworkers.[43] This is further evidenced in the He−I measurements, when the lower penetration depth reveals a VBM of 3.25 eV, with a Fermi level just 0.15 eV away from the conduction band of bulk GaN (E_g = 3.4 eV), pointing toward the presence of surface contaminant. Note that these drastic changes in VBM can result even if the contaminants are below the detection limit of XPS,[43] which is likely the case in our samples as discussed later. Samples containing the porous GaN film show markedly different VBM and Φ_S values in comparison to the reference GaN substrate. Φ_S of porous GaN lies in a narrow range of 4.52−4.64 eV with no clear correlation to deposition time. The presence of adsorbed oxygen has been associated with changes in Φ_S for related materials.[44−47] On the other hand, the VBM shows a clear reduction with a longer growth time, decreasing from 3.74 to 2.83 eV. The significantly larger VBM in samples with only 15 and 30 min of deposition time strongly suggests the presence of additional donor states. It is known that the valence band spectra of GaN are governed by hybridized states (N 2p-Ga-4p, N-2p-Ga 4s, N 2p-Ga 4s, and mixed orbitals) and satellite peaks.[32,48−50] Therefore, the VBM position is mostly affected by the density of the N−Ga states. Hawkridge and Cherns[51] reported that oxygen can accumulate at the pit surfaces and substitute the nitrogen that is exposed at the $(10\bar{1}1)$ facet. The introduction of oxygen can eventually generate donor states, causing the observed increase in VBM. XPS measurements discussed in the following section support the correlation to the density of the N−Ga states by the existence of nonstoichiometric GaN_xO_y observed in samples with 15 and 30 min of deposition time. For samples with a deposition time of 45 and 60 min, the VBM reduces and approaches that of the *p*-type GaN substrate, with a difference of only 0.27 eV between the 60 min porous GaN and the GaN substrate. This difference could be related to a higher content of contaminants (oxygen/hydroxides) on the porous GaN due to the new crystal surfaces exposed and to the larger surface area due to the porous nature.

Surface Characteristics. The elemental composition and chemical states of the surface of the porous GaN films were characterized by XPS. Figure 6a shows the high-resolution XPS of Ga(3d) for samples at different growth times with a mean feature centered at a BE of ∼20.0 eV.[52] The Ga (3d) spectra were deconvoluted in three peaks attributed to different chemical bonds: the first peak at ∼18.1 eV related to Ga−Ga bonding, a second at ∼19.6 eV attributed to the Ga−N states, and a third peak at ∼21.0 eV which corresponds to Ga−O states.[52] Note that the Ga−Ga feature is observed only for the lowest growth time (15 min), likely due to an incomplete formation of a GaN film. The BE of the Ga−N peak shifts from

https://doi.org/10.1021/acs.jpcc.3c05878
J. Phys. Chem. C 2023, 127, 24658−24665

19.6 to 20.2 eV with increasing deposition time, while the Ga−O states appear only for samples grown at 30, 45, and 60 min with similar intensity. A comparison between Ga−N and Ga−O states is shown in Figure 7a. According to the literature, the

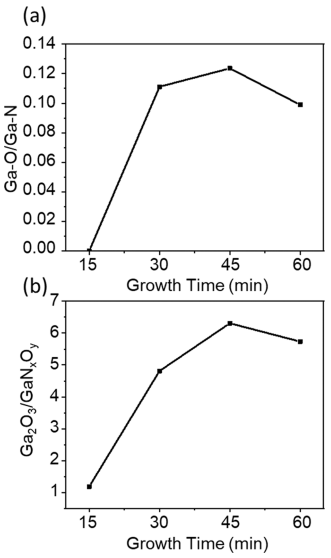

Figure 7. Ratio among (a) Ga−O and Ga−N and (b) Ga_2O_3 and GaN_xO_y chemical states for the samples grown at different deposition times.

Ga−O states can be attributed to Ga_2O_3,[53] while the shift in the peak energy is a strong indication of the presence of band bending in the surface which affects the electronic properties due to the presence of different surface states.[32]

The XPS region around the O-1s BE is shown in Figure 6b. The deconvolution of the spectra shows three peaks at BE values of 530.2, 531.6, and 533.2 eV corresponding to the chemical states of GaN_xO_y, Ga_2O_3, and hydroxyl species (−OH), respectively.[52] A decrease in the contribution from 42 to 13% of GaN_xO_y states with time is observed, while Ga_2O_3 states increase from 50 to 82% (from 15 to 45 min of deposition time), indicating a clear increase in Ga oxides at the surfaces of the V-pits. Note that there is a slight reduction of oxide states to 80% for a growth time of 60 min. The last observation could indicate that the size of the V-pits limits the amount of oxygen coverage inside the pits. The changes between Ga_2O_3 and GaN_xO_y are easily observed in Figure 7b, where the Ga_2O_3/GaN_xO_y ratio increases with the deposition time.

The deconvolution of states in the N (1s) spectra is shown in Figure 6c, where three peaks are observed at BE values of 396.8, 398.1, and 399.2 eV corresponding to N−Ga, N−H, and N−O, respectively. The features not resolved in Figure 6c; corresponding to energies <396.2 eV (marked with an arrow), are related to Ga LMM Auger transition corresponding to electron transitions between different energy levels, these can reveal different chemical environments seen in the porous GaN films, where the presence of GaO_xN_y has shown suppressed Auger transitions,[54] in agreement with our XPS results. Besides the N−Ga states, we found features corresponding to N−O and N−H states that slightly fade away with the growth time. At 15 min of deposition time, there is a significant contribution of nitrogen bonded to hydrogen which likely originates from the partial decomposition of the NH_3 gas, while the nitrogen−oxygen states could be related to the presence of non-stoichiometric GaN_xO_y as seen in the O (1) spectrum. At 60 min of growth time, the porous film consists mostly of GaN and Ga_2O_3, with some remanent of GaN_xO_y.

We performed DFT simulations to investigate the feasibility of forming oxidized species (e.g., Ga_2O_3, GaN_xO_y) onto GaN. We evaluated the adsorption energy of oxygen (E_O^{ads}) relative to $O_{2(gas)}$ on the surface of two crystallographic surfaces seen in the V-pits, namely, Ga-terminated (0001) and the $(\bar{1}011)$ as indicated in Figure 1d. The E_O^{ads} values were obtained using periodic (0001) and $(\bar{1}011)$ surfaces without considering edge effects, and their values are shown in Figure 8 as guidance (see

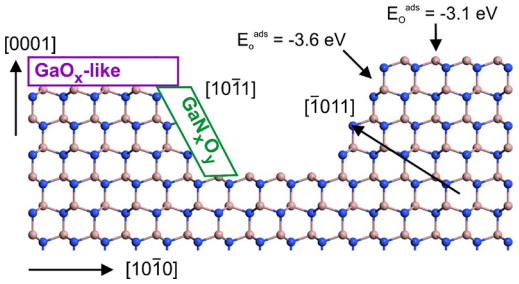

Figure 8. Schematic configuration of a V-pit in GaN showing the crystal planes involved in its formation. The oxygen adsorption energies (E_O^{ads}) were obtained using periodic surfaces and are stated here as guidance.

the experimental section for further details). The E_O^{ads} values on both Ga-terminated (0001) and N-terminated $(\bar{1}011)$ surfaces have relatively similar values of −3.1 and −3.6 eV, respectively. Note that negative E_O^{ads} indicates favorable oxygen adsorption. The magnitude of E_O^{ads} indicates a strong interaction between the oxygen with Ga and N on both surfaces, eventually leading to the formation of the experimentally observed GaN_xO_y and Ga_2O_3, in agreement with the XPS and UPS measurements. This information is depicted in Figure 8, where an idealized atomic model of a V-pit in the Ga-terminated (0001) surface is shown, indicating the plausible origins of GaN_xO_y and Ga_2O_3.

CONCLUSIONS

Crystalline and porous gallium nitride films were deposited by the chemical vapor deposition technique onto a *p*-type GaN/undoped-GaN/sapphire substrate at different growth times due to the reaction of metallic Ga and NH_3. We have observed a clear relation between the deposition time used with the thickness, morphology, and optical and electronic properties exhibited for the films obtained. An interesting finding is the presence of V-pits orientated along the [0001] direction of GaN, in which these V-pits can significantly modify the surface and electronic properties of the material. Our DFT calculations show that the main crystallographic planes observed in the V-pits present a high adsorption energy for oxygen, being this the main reason for the change in size with the deposition time due to the formation of oxygen-rich phases such as Ga_2O_3 and nonstoichiometric GaN_xO_y on the inner surface of V-pits. We can conclude that the change in the ratio of the Ga_2O_3 and GaN_xO_y phases with time, as indicated by the XPS results, strongly modifies the work function and the VBM experimentally measured by UPS. On the other hand, the decrease observed in the optical band gap of the porous films is more related to changes in the tensile strain introduced by the presence of open-core screw dislocations rather than the lattice

https://doi.org/10.1021/acs.jpcc.3c05878
J. Phys. Chem. C 2023, 127, 24658−24665

mismatch and differences in thermal expansion coefficients between the GaN and the sapphire substrate. We have also supported this result with DFT calculations, and the good correlation between the experimental and theoretical data opens the possibility for fine-tuning the material's optical properties depending on the needs. We believe that the detailed study presented in this work not only shows the intricate relation between surface states and electronic properties of semiconducting materials but also gives clear directions for the design of GaN heterojunctions with specific optical and electronic properties as required, as an example, on different kinds of electronics components.

■ ASSOCIATED CONTENT

Supporting Information

The Supporting Information is available free of charge at https://pubs.acs.org/doi/10.1021/acs.jpcc.3c05878.

Ultra-high vacuum system; parameters for UPS measurements; mean pore size; optical band gaps; DFT-HSE electronic band gap; and UPS spectra (PDF)

■ AUTHOR INFORMATION

Corresponding Authors

Thomas Wågberg − *Department of Physics, Umeå University, SE-901 87 Umeå, Sweden;* orcid.org/0000-0002-5080-8273; Phone: +4690 786 5993; Email: thomas.wagberg@umu.se

Eduardo Gracia-Espino − *Department of Physics, Umeå University, SE-901 87 Umeå, Sweden;* orcid.org/0000-0001-9239-0541; Phone: +4690 786 6339; Email: eduardo.gracia@umu.se

Authors

Vladimir Miranda La Hera − *Department of Physics, Umeå University, SE-901 87 Umeå, Sweden*

Josué Mena − *Department of Physics, Umeå University, SE-901 87 Umeå, Sweden; Departament de Química Física i Inorganica, Universitat Rovira i Virgili, 43007 Tarragona, Spain;* orcid.org/0000-0003-4368-0651

Esdras Josué Canto-Aguilar − *Department of Physics, Umeå University, SE-901 87 Umeå, Sweden;* orcid.org/0009-0003-9618-3162

Hamid Reza Barzegar − *Department of Physics, Umeå University, SE-901 87 Umeå, Sweden*

Joan J. Carvajal − *Departament de Química Física i Inorganica, Universitat Rovira i Virgili, 43007 Tarragona, Spain;* orcid.org/0000-0002-4389-7298

Complete contact information is available at: https://pubs.acs.org/10.1021/acs.jpcc.3c05878

Author Contributions

[§]V.M.L.H. and J.M. contribution as a first author.

Notes

The authors declare no competing financial interest.

■ ACKNOWLEDGMENTS

We acknowledge support from Vetenskapsrådet (2018-03937 and 2021-04629), Energimyndigheten (45419-1), the Swedish Foundation for Strategic Research (SSF-Agenda 2030-PUSH), and the Carl Tryggers Foundation (CTS 21-1581). The computations were enabled by resources provided by the National Academic Infrastructure for Supercomputing in Sweden (NAISS) at the National Supercomputer Centre (NSC) in Linköping University partially funded by the Swedish Research Council through grant agreement no. 2022-06725. We also thank the Umeå Core Facility for Electron Microscopy (UCEM), the Vibrational Spectroscopy Core Facility (ViSp), the NanoLab platform, and the XPS platform at Umeå University.

■ REFERENCES

(1) Kibria, M. G.; Zhao, S.; Chowdhury, F. A.; Wang, Q.; Nguyen, H. P.; Trudeau, M. L.; Guo, H.; Mi, Z. Tuning the surface Fermi level on p-type gallium nitride nanowires for efficient overall water splitting. *Nat. Commun.* **2014**, *5*, 3825.

(2) Pu, T.; Younis, U.; Chiu, H. C.; Xu, K.; Kuo, H. C.; Liu, X. Review of Recent Progress on Vertical GaN-Based PN Diodes. *Nanoscale Res. Lett.* **2021**, *16*, 101.

(3) Iida, D.; Ohkawa, K. Recent progress in red light-emitting diodes by III-nitride materials. *Semicond. Sci. Technol.* **2022**, *37*, No. 013001.

(4) Najar, A.; Gerland, M.; Jouiad, M. Porosity-induced relaxation of strains in GaN layers studied by means of micro-indentation and optical spectroscopy. *J. Appl. Phys.* **2012**, *111*, No. 093513.

(5) Sato, T.; Kumazaki, Y.; Kida, H.; Watanabe, A.; Yatabe, Z.; Matsuda, S. Large photocurrents in GaN porous structures with a redshift of the photoabsorption edge. *Semicond. Sci. Technol.* **2016**, *31*, No. 014012.

(6) Yao, Y. X.; Liang, Y.; Guo, J. B.; Xiu, H. X. The development and applications of nanoporous gallium nitride in optoelectronics: a review. *Semicond. Sci. Technol.* **2023**, *38*, No. 074001.

(7) Pasayat, S. S.; Wu, F.; Gupta, C.; Denbaars, S. P.; Nakamura, S.; Keller, S.; Mishra, U. K. Study of Pore Geometry and Dislocations in Porous GaN Based Pseudo-Substrates Using TEM. *IEEE J. Quantum Electron.* **2022**, *58*, 1.

(8) Mokhov, E. N.; Wolfson, A. A., Growth of AlN and GaN crystals by sublimation. In *Single Crystals of Electronic Materials*; Fornari, R., Ed.; Woodhead Publishing, 2019; p 401.

(9) Lee, C. D.; Feenstra, R. M.; Shigiltchoff, O.; Devaty, R. P.; Choyke, W. J. Structural properties of GaN films grown by molecular beam epitaxy on singular and vicinal 6H-SiC(0001). *MRS Internet J. Nitride Semicond. Res.* **2002**, *7*, No. e2.

(10) Strite, S.; Morkoç, H. GaN, AlN, and InN: A review. *J. Vac. Sci. Technol. B* **1992**, *10*, 1237.

(11) Choy, K. L. Chemical vapour deposition of coatings. *Prog. Mater. Sci.* **2003**, *48*, 57.

(12) Carlsson, J.-O.; Martin, P. *Chemical Vapor Deposition*, 2010; pp 314.

(13) Mena gomez, J.; Carvajal, J. J.; Bilousov, O.; Diaz, F.; Aguilo, M. Investigation of antireflective and hydrophobic properties in polycrystalline GaN films with dual porosity produced by CVD. *Sci. Rep.* **2019**, *9*, 11686.

(14) Song, Y. M.; Choi, E. S.; Park, G. C.; Park, C. Y.; Jang, S. J.; Lee, Y. T. Disordered antireflective nanostructures on GaN-based light-emitting diodes using Ag nanoparticles for improved light extraction efficiency. *Appl. Phys. Lett.* **2010**, *97*, No. 093110.

(15) Lu, L.; Gao, Z. Y.; Shen, B.; Xu, F. J.; Huang, S.; Miao, Z. L.; Hao, Y.; Yang, Z. J.; Zhang, G. Y.; Zhang, X. P.; et al. Microstructure and origin of dislocation etch pits in GaN epilayers grown by metal organic chemical vapor deposition. *J. Appl. Phys.* **2008**, *104*, 123525.

(16) Gao, Z. Y.; Xue, X. W.; Li, J. J.; Wang, X.; Xing, Y. H.; Cui, B. F.; Zou, D. S. Understanding of surface pit formation mechanism of GaN grown in MOCVD based on local thermodynamic equilibrium assumption. *Chin. Physics B* **2016**, *25*, No. 066105.

(17) Besendörfer, S.; Meissner, E.; Tajalli, A.; Meneghini, M.; Freitas, J. A.; Derluyn, J.; Medjdoub, F.; Meneghesso, G.; Friedrich, J.; Erlbacher, T. Vertical breakdown of GaN on Si due to V-pits. *J. Appl. Phys.* **2020**, *127*, No. 015701.

(18) Koike, K.; Lee, S.; Cho, S. R.; Park, J.; Lee, H.; Ha, J. S.; Hong, S. K.; Lee, H. Y.; Cho, M. W.; Yao, T. Improvement of Light Extraction Efficiency and Reduction of Leakage Current in GaN-

Based LED via V-Pit Formation. *IEEE Photonics Technol. Lett.* **2012**, *24*, 449.
(19) Zhou, S.; Liu, X.; Yan, H.; Gao, Y.; Xu, H.; Zhao, J.; Quan, Z.; Gui, C.; Liu, S. The effect of nanometre-scale V-pits on electronic and optical properties and efficiency droop of GaN-based green light-emitting diodes. *Sci. Rep.* **2018**, *8*, 11053.
(20) Elsner, J.; Gutierrez, R.; Hourahine, B.; Jones, R.; Haugk, M.; Frauenheim, T. A theoretical study of O chemisorption on GaN (0001)/(000(1)over-bar) surfaces. *Solid State Commun.* **1998**, *108*, 953.
(21) Bermudez, V. M. Study of oxygen chemisorption on the GaN(0001)-(1 × 1) surface. *J. Appl. Phys.* **1996**, *80*, 1190.
(22) Bilousov, O. V.; Carvajal, J. J.; Geaney, H.; Zubialevich, V. Z.; Parbrook, P. J.; Martinez, O.; Jimenez, J.; Diaz, F.; Aguilo, M.; O'dwyer, C. Fully porous GaN p−n junction diodes fabricated by chemical vapor deposition. *ACS Appl. Mater. Interfaces* **2014**, *6*, 17954.
(23) Bilousov, O. V.; Carvajal, J. J.; Mena, J.; Martínez, O.; Jiménez, J.; Geaney, H.; Díaz, F.; Aguiló, M.; O'dwyer, C. Epitaxial growth of (0001) oriented porous GaN layers by chemical vapour deposition. *CrystEngComm* **2014**, *16*, 10255.
(24) Giannozzi, P.; Andreussi, O.; Brumme, T.; Bunau, O.; Buongiorno nardelli, M.; Calandra, M.; Car, R.; Cavazzoni, C.; Ceresoli, D.; Cococcioni, M.; et al. Advanced capabilities for materials modelling with Quantum ESPRESSO. *J. Phys.: Condens. Matter* **2017**, *29*, 465901.
(25) Giannozzi, P.; Baroni, S.; Bonini, N.; Calandra, M.; Car, R.; Cavazzoni, C.; Ceresoli, D.; Chiarotti, G. L.; Cococcioni, M.; Dabo, I.; et al. QUANTUM ESPRESSO: a modular and open-source software project for quantum simulations of materials. *J. Phys.: Condens. Matter* **2009**, *21*, No. 395502.
(26) Troullier, N.; Martins, J. L. Efficient pseudopotentials for plane-wave calculations. *Phys. Rev. B Condens. Matter.* **1991**, *43*, 1993.
(27) Heyd, J.; Scuseria, G. E.; Ernzerhof, M. Hybrid functionals based on a screened Coulomb potential. *J. Chem. Phys.* **2003**, *118*, 8207.
(28) Heying, B.; Averbeck, R.; Chen, L. F.; Haus, E.; Riechert, H.; Speck, J. S. Control of GaN surface morphologies using plasma-assisted molecular beam epitaxy. *J. Appl. Phys.* **2000**, *88*, 1855.
(29) Kisielowski, C.; Kruger, J.; Ruvimov, S.; Suski, T.; Ager, J. W., 3rd; Jones, E.; Liliental-weber, Z.; Rubin, M.; Weber, E. R.; Bremser, M. D.; et al. Strain-related phenomena in GaN thin films. *Phys. Rev. B Condens. Matter.* **1996**, *54*, 17745.
(30) Mena, J.; Carvajal, J. J.; Martinez, O.; Jimenez, J.; Zubialevich, V. Z.; Parbrook, P. J.; Diaz, F.; Aguilo, M. Optical and structural characterisation of epitaxial nanoporous GaN grown by CVD. *Nanotechnology* **2017**, *28*, 375701.
(31) Kim, J. B.; H, K. Characterization of hexagonal defects in gallium nitride on sapphire. *J. Ceram. Process. Res.* **2007**, *8*, 277.
(32) Mishra, M.; Krishna, T. C. S.; Aggarwal, N.; Kaur, M.; Singh, S.; Gupta, G. Pit assisted oxygen chemisorption on GaN surfaces. *Phys. Chem. Chem. Phys.* **2015**, *17*, 15201.
(33) Wan, K. S.; Porporati, A. A.; Feng, G.; Yang, H.; Pezzotti, G. Biaxial stress dependence of the electrostimulated near-band-gap spectrum of GaN epitaxial film grown on (0001) sapphire substrate. *Appl. Phys. Lett.* **2006**, *88*, 251910.
(34) Peng, H. Y.; Mccluskey, M. D.; Gupta, Y. M.; Kneissl, M.; Johnson, N. M. Shock-induced band-gap shift in GaN: Anisotropy of the deformation potentials. *Phys. Rev. B Condens. Matter.* **2005**, *71*, No. 115207.
(35) Garza, A. J.; Scuseria, G. E. Predicting Band Gaps with Hybrid Density Functionals. *J. Phys. Chem. Lett.* **2016**, *7*, 4165.
(36) Abdalla, A. S.; Khan, M. S.; Alameen, S.; Eisa, M. H.; Aldaghri, O. Electronic and magnetic properties of Fe-doped GaN: first-principle calculations. *Z. Naturforsch. A* **2021**, *76*, 245.
(37) Kaewmeechai, C.; Laosiritaworn, Y.; Jaroenjittichai, A. P. HSE hybrid functional calculation of band gap deformation potential in MgGeN2. *J. Phys.: Conf. Ser.* **2018**, *1144*, No. 012045.
(38) Chatzopoulou, P.; Vasileiadis, I. G.; Komninou, P.; Pontikis, V.; Karakostas, T.; Dimitrakopulos, G. P. Strain-Induced Band Gap Variation in InGaN/GaN Short Period Superlattices. *Crystals* **2023**, *13*, 700.
(39) Ping, Y.; Galli, G.; Goddard, W. A. Electronic Structure of IrO: The Role of the Metal d Orbitals. *J. Phys. Chem. C* **2015**, *119*, 11570.
(40) Duhm, S. Interface energetics in organic electronic devices. In *Organic Flexible Electronics*, Cosseddu, P.; Caironi, M., Eds.; Woodhead Publishing, 2021; p 143.
(41) Smith, G. C. Quantitative Surface Microanalysis by Auger and X-Ray Photoelectron-Spectroscopy. *Mater. Charact.* **1990**, *25*, 37.
(42) Helander, M. G.; Wang, Z. B.; Qiu, J.; Greiner, M. T.; Puzzo, D. P.; Liu, Z. W.; Lu, Z. H. Chlorinated indium tin oxide electrodes with high work function for organic device compatibility. *Science* **2011**, *332*, 944.
(43) Tracy, K. M.; Mecouch, W. J.; Davis, R. F.; Nemanich, R. J. Preparation and characterization of atomically clean, stoichiometric surfaces of n- and p-type GaN(0001). *J. Appl. Phys.* **2003**, *94*, 3163.
(44) Parker, D. H.; Bartram, M. E.; Koel, B. E. Study of High Coverages of Atomic Oxygen on the Pt(111) Surface. *Surf. Sci.* **1989**, *217*, 489.
(45) Zhao, J. P.; Xu, Y. L.; Liu, S. H.; Ding, X. D. The effect of oxygen-containing species on corrosion behavior of Ta (110) surface: A DFT study with an experimental verification. *Appl. Surf. Sci.* **2022**, *586*, No. 152810.
(46) Maeng, M.; Kim, J. H.; Hong, J. A.; Park, Y. Effects of oxygen plasma treatments on the work function of indium tin oxide studied by photoelectron spectroscopy. *J. Korean Phys. Soc.* **2016**, *68*, 692.
(47) Malek, A.; Eikerling, M. H. Chemisorbed Oxygen at Pt(111): a DFT Study of Structural and Electronic Surface Properties. *Electrocatalysis* **2018**, *9*, 370.
(48) Skuridina, D.; Dinh, D. V.; Lacroix, B.; Ruterana, P.; Hoffmann, M.; Sitar, Z.; Pristovsek, M.; Kneissl, M.; Vogt, P. Polarity determination of polar and semipolar (11(2)over-bar2) InN and GaN layers by valence band photoemission spectroscopy. *J. Appl. Phys.* **2013**, *114*, 173503.
(49) Veal, T. D.; King, P. D. C.; Jefferson, P. H.; Piper, L. F. J.; Mcconville, C. F.; Lu, H.; Schaff, W. J.; Anderson, P. A.; Durbin, S. M.; Muto, D.; et al. In adlayers on c-plane InN surfaces: A polarity-dependent study by x-ray photoemission spectroscopy. *Phys. Rev. B Condens. Matter.* **2007**, *76*, No. 075313.
(50) Magnuson, M.; Mattesini, M.; Höglund, C.; Birch, J.; Hultman, L. Electronic structure of GaN and Ga investigated by soft x-ray spectroscopy and first-principles methods. *Phys. Rev. B Condens. Matter.* **2010**, *81*, No. 085125.
(51) Hawkridge, M. E.; Cherns, D. Oxygen segregation to dislocations in GaN. *Appl. Phys. Lett.* **2005**, *87*, 221903.
(52) Li, D. S.; Sumiya, M.; Fuke, S.; Yang, D. R.; Que, D. L.; Suzuki, Y.; Fukuda, Y. Selective etching of GaN polar surface in potassium hydroxide solution studied by x-ray photoelectron spectroscopy. *J. Appl. Phys.* **2001**, *90*, 4219.
(53) Moldovan, G.; Roe, M. J.; Harrison, I.; Kappers, M.; Humphreys, C. J.; Brown, P. D. Effects of KOH etching on the properties of Ga-polar n-GaN surfaces. *Philos. Mag.* **2006**, *86*, 2315.
(54) Su, L. X.; Chen, S. Y.; Zhao, L. Q.; Zuo, Y. Q.; Xie, J. Low temperature atomic layer deposition of GaOxNy thin film on III-GaN:Mg for UV photodetector. *Appl. Phys. Lett.* **2020**, *117*, 211101.

https://doi.org/10.1021/acs.jpcc.3c05878
J. Phys. Chem. C 2023, 127, 24658−24665